Supplementary information

Ligand-Engineered Synthesis of Carbon Encapsulated Ni Nanoparticles for Efficient Alkaline Hydrogen Oxidation Reaction

Yanan Chen[a], Aiqing Cao[b], Yongsheng Wang[a], Jiaxin Wang[a], Hao Wang[a], Qingqing Lv[a], Shuxin Zhang[a], Chengjin Chen[a], Yaping Li[b], Wei Zhu[a,c] and Zhongbin Zhuang[a,c]

[a]State Key Lab of Organic-Inorganic Composites and Beijing Advanced Innovation Center for Soft Matter Science and Engineering, Beijing University of Chemical Technology, Beijing 100029, China.

[b]State Key Laboratory of Chemical Resource Engineering, College of Chemistry, Beijing University of Chemical Technology, Beijing 100029, China.

[c]Beijing Key Laboratory of Intelligent Design and Manufacturing for Hydrogen Energy Materials, Beijing University of Chemical Technology, Beijing, 100029, China.

Materials.

Nickel (II) nitrate hexahydrate ($Ni(NO_3)_2 \cdot 6H_2O$) was purchased from China medicine Shanghai chemical reagent corporation. Pyridine-3-amidoxime (Py-3-AO), pyridine-2-amidoxime (Py-2-AO), pyridine-4-amidoxime (Py-4-AO), pyrazine-2-amidoxime (Pa-3-AO), pyridine-3-aldoxime (Py-3-O), triethylamine (TEA), urea, citric acid (CA), and ethanol were obtained from Aladdin. 2-amino-pyridine-3-carbaldehyde oxime hydrochloride (Py-2A-3O) was purchased from Adamas. The hydroxide exchange membrane (PiperION™ A20) and the ionomer were bought from Versogen. Ultrapure water (18.2 MΩ·cm, Mili-Q, Merck) was used in the synthesis of catalysts and electrochemical measurements.

Methods

Synthesis of carbon encapsulated Ni catalysts

In the typical synthesis of the Ni-Py-3-AO catalyst, 1163 mg of $Ni(NO_3)_3 \cdot 6H_2O$ was dissolved in 20 mL of ethanol to form Solution A. Separately, 548 mg of Py-3-AO was dissolved in 10 mL of ethanol to form Solution B. Solution A was added dropwise to Solution B under stirring at room temperature. Then, 1 mL of triethylamine was added to the solution. The mixture was stirred for 2 hours. The resulting solid was isolated by centrifugation, washed, and dried at 80 °C in an oven to obtain the precursor.

The precursor (200 mg) was subjected to calcination at 500 °C for 2 hours under 5% H_2 and 95% Ar atmosphere in a tubular furnace to obtain the Ni-Py-3-AO catalyst. The resulting catalyst was stored in isopropanol.

The Ni-Py-2-AO, Ni-Py-4-AO, Ni-Pa-3-AO, Ni-Py-3-O and Ni-Py-2A-3O were synthesized following a similar procedure but adding the corresponding ligands.

Synthesis of the Ni/C.

300 mg of Ketjen black was dispersed in 15 mL of ethanol in a round-bottom flask, and the slurry was magnetically stirred for 30 min. 3.57 g of $Ni(NO_3)_2 \cdot 6H_2O$, 0.023 g of urea and 0.207 g of citric acid monohydrate were dissolved in 3 mL of deionized water. Then, the solution was added to the carbon slurry dropwise. The obtained slurry was magnetically stirred for 10 h at room temperature and then dried at 80 °C in an oven. Finally, it was placed in a furnace and calcinated at 470 °C for 1 h under the atmosphere of 5% H_2 and 95% Ar with a gas flow rate of 50 sccm.

Physical characterizations

X-ray diffraction (XRD) patterns were collected using a Rigaku D/Max 2500 VB2+/PC diffractometer with Cu Kα radiation (λ = 0.154 nm). Transmission electron microscopy (TEM) images were acquired on a Hitachi HT7700 microscope operated at an accelerating voltage of

100 kV. High-resolution transmission electron microscopy (HRTEM) characterization was performed using an FEI Talos F200X transmission electron microscope equipped with a SUPER X energy-dispersive X-ray spectroscopy (EDS) system. X-ray photoelectron spectroscopy (XPS) analysis was performed using a Thermo Fisher Scientific Nexsa XPS system. Inductively coupled plasma mass spectrometry (ICP-MS) analysis was performed using an Agilent 7800 ICP-MS system for quantitative elemental composition determination.

Electrochemical measurements：

Electrochemical measurements were performed using a CHI760 electrochemical workstation coupled with a Pine Research rotating disk electrode (RDE) system. A 0.1 M KOH aqueous solution served as the electrolyte. All experiments were conducted at 30 °C.

The glassy carbon (GC) working electrode was polished with alumina polishing powder and thoroughly rinsed with deionized water prior to use. Catalyst ink was prepared by dispersing 3 mg of catalyst in a mixture of 886 µL isopropanol, 99 µL deionized water, and 15 µL Nafion solution (5 wt %, DuPont). The mixture was ultrasonicated for 1 hour in an ice-water bath to ensure homogeneity. 15 µL of the well-dispersed catalyst ink was deposited onto the polished GC electrode surface and dried at room temperature, yielding a catalyst loading of 230 µg cm^{-2}. For comparison, a commercial Pt/C (20 wt %, Premetek) catalyst ink was prepared with a Pt loading of 5 µg cm^{-2}. Similarly, 15 µL of this ink was deposited onto a separate GC electrode. A Hg/HgO (1 M KOH) electrode was used as the reference electrode. A gold wire served as the counter electrode. All measured potentials were referenced to the reversible hydrogen electrode (RHE). The RHE calibration was performed in H_2-saturated 0.1 M KOH using a Pt/C electrode, determining the equilibrium potential for the hydrogen oxidation/evolution reactions (HOR/HER). Linear sweep voltammograms were recorded at a scan rate of 1 mV s^{-1}. All LSV data were *iR*-compensated. EIS measurements were conducted over a frequency range of 100 kHz to 1 Hz. An AC amplitude of 10 mV was applied.

Electrochemical in situ ATR-SEIRAS test

The in-situ ATR-SEIRAS experiments were conducted using a Nicolet iS50 FT-IR spectrometer equipped with a MCT detector and a PIKE VeeMAX III variable-angle ATR sampling accessory for ATR testing. The spectral resolution was set at 4 cm^{-1}, and each spectrum was obtained by averaging 64 collected spectra. A single-crystal silicon wafer with an incident angle of 60° was used as the reflective element. After cleaning its surface, a gold film was chemically deposited on it to enhance infrared absorption and facilitate electron conduction. The catalysts were formulated into ink and spin-coated onto the Au film to serve as the working electrode for the SEIRAS experiment. The working electrode was placed in an in-situ spectroelectrochemical cell, with a Pt wire as the counter electrode and a Hg/HgO electrode as the reference electrode. SEIRAS spectra were collected in a stepwise manner within the potential range

from 0.15 to −0.15 V (vs. RHE). The background spectrum was collected at 0.2 V. The spectra were defined in terms of absorbance as Abs = $-\lg(R/R_0)$, where R and R_0 represent the reflected infrared intensities of the sample and background single-beam spectra, respectively.

MEA tests：

The anode catalyst (Ni-Py-3-AO or Ni/C) and cathode catalyst (40% commercial Pt/C) ink were prepared by dispersion the catalysts in the corresponding catalyst with ionomer (TP-100) in isopropyl alcohol and deionized water under ultrasonic treatments. The inks were then uniformly spray-coated onto both sides of an alkaline exchange membrane (AEM) using an air spray gun, forming a catalyst-coated membrane (CCM). The active area of the membrane was 5 cm^2. The metal loadings were controlled at 3 mg_{Ni} cm^{-2} (anode) and 0.4 mg_{Pt} cm^{-2} (cathode). The ionomer content was adjusted to achieve an ionomer-to-carbon ratio (I/C) of 0.6. The prepared CCM was immersed in 1 M KOH solution for 3 hours to facilitate anion exchange within the membrane, replacing the original anions with OH^-. Then CCM was assembled into a single fuel cell. Fuel cell performance was evaluated using a Scribner 850e fuel cell test station. The cell temperature was maintained at 95 °C. The anode was fed with 90 °C humidified H_2, and the cathode was fed with 95 °C humidified O_2. The flow rates of H_2 and O_2 were 500 sccm, and the gas back pressure was set at 250 kPa. When testing stability, the cell, anode and cathode temperatures were maintained at 80, 78, and 80 °C, respectively. The flow rate of H_2 and O_2 was 300 sccm each, and the gas back pressure was set at 100 kPa.

Computational details

The calculations in this work were performed based on the first principles method of density functional theory (DFT) using the Vienna Ab initio Simulation Package (VASP) software package.[1] The Perdew-Burke-Ernzerhof (PBE) generalised gradient approximation (GGA) was used to calculate the exchange and associated energy density functions.[2,3] The cutoff energy was set to 450 eV and the energy convergence precision was 10^{-4} eV. The Brillouin zone was sampled using the Monkhorst scheme with 2 × 2 × 1 k-point mesh for Ni, Ni@C-1N, and Ni@C-2N.The catalyst models were constructed by encapsulating Ni nanoparticles with graphene layers, forming Ni@C, Ni@C-1N, and Ni@C-2N configurations. Then the 15 Å vacuum was employed with in the z axis to prevent periodic image interactions between neighboring slabs. During geometry optimization, all atoms except those in the bottom layer were allowed to relax, and the atomic positions were optimized until the forces were less than 0.03 eV/Å. Then, we selected Ni as the active site for the hydrogen oxidation reaction (HOR) process. The adsorption free energy of the reaction intermediates is calculated using Equation (1):[4]

$$\Delta G_{ads} = E_{ads+sub} - E_{sub} - E_{ads} + \Delta E_{ZPE} - T\Delta S \quad (1)$$

where ads = H, $E_{ads+sub}$ is the energy of intermediate adsorbed on the surface structure, E_{sub} is the energy of substrate, E_{ads} is the energy of adsorbate, ΔE_{ZPE} is the zero-point energy change, and ΔS is the entropy change. In this work, the values of ΔE_{ZPE} and ΔS were obtained by vibration frequency calculation. Here, T is the temperature, and it was set to 298.15 K during the calculations.

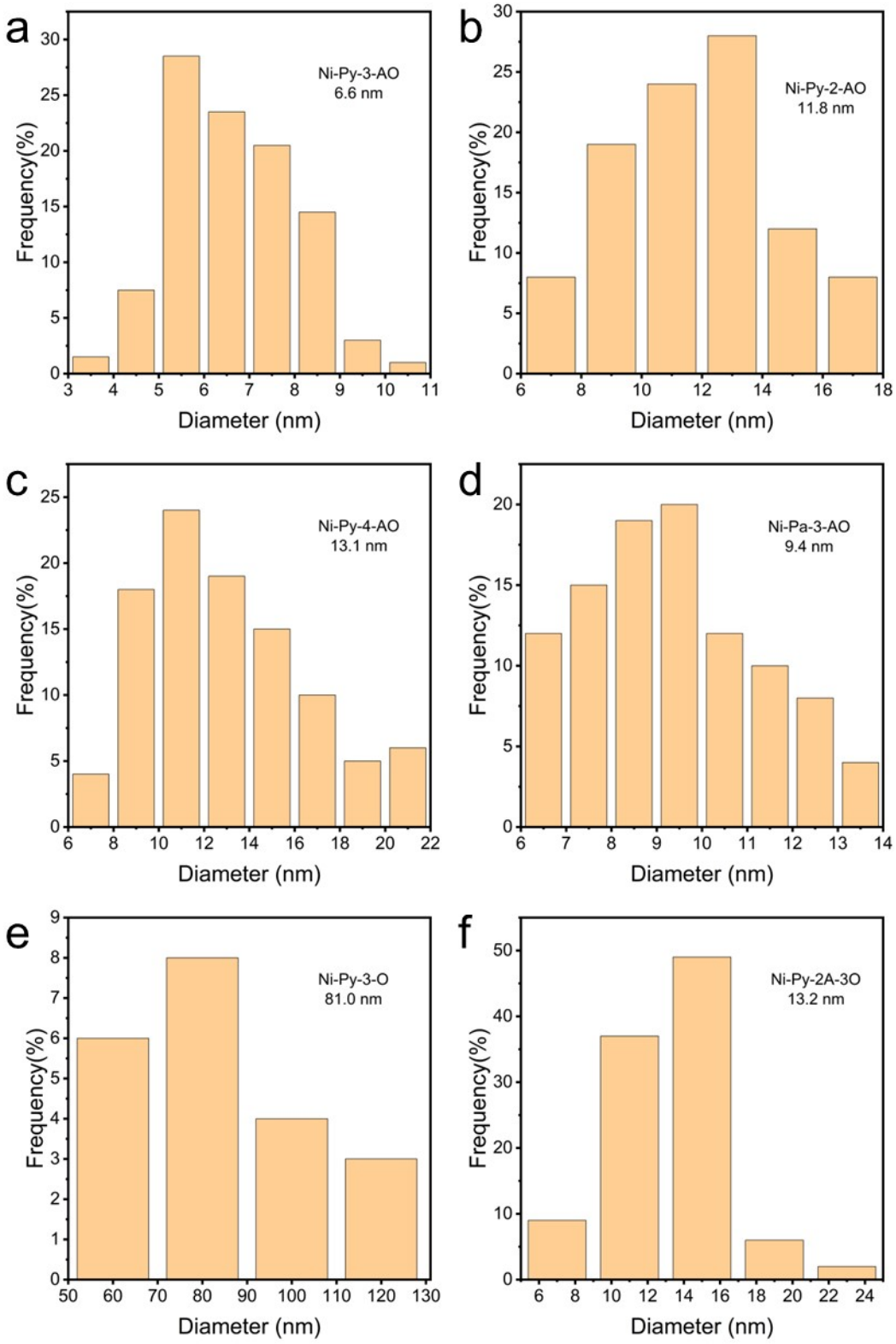

Figure S1. Size distribution of (a) Ni-Py-3-AO, (b) Ni-Py-2-AO, (c) Ni-Py-4-AO, (d) Ni-Pa-3-AO, (e) Ni-Py-3-O and (f) Ni-Py-2A-3O.

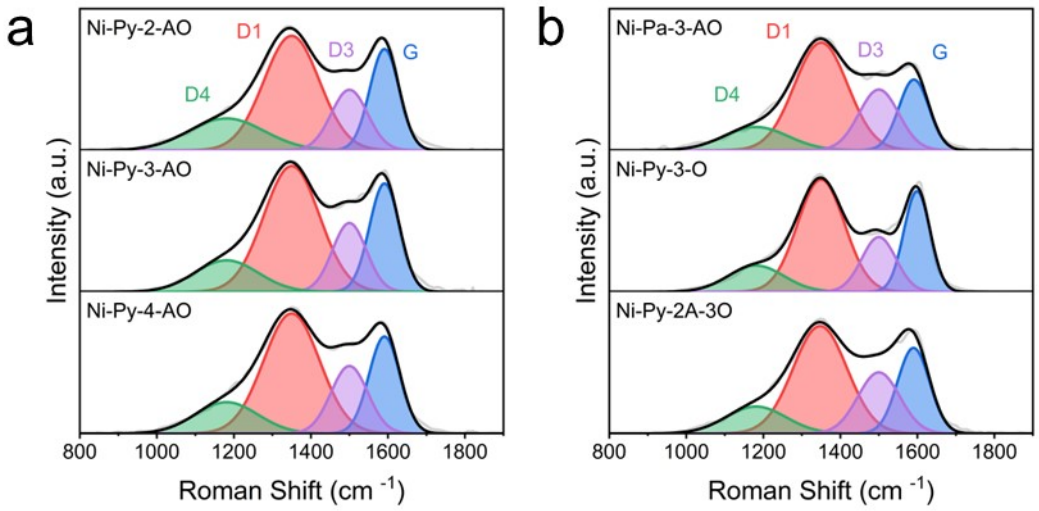

Figure S2. (a) Raman spectra of Ni-Py-2-AO, Ni-Py-3-AO and Ni-Py-4-AO. (b) Raman spectra of Ni-Pa-3-AO, Ni-Py-3-O and Ni-Py-2A-3O.

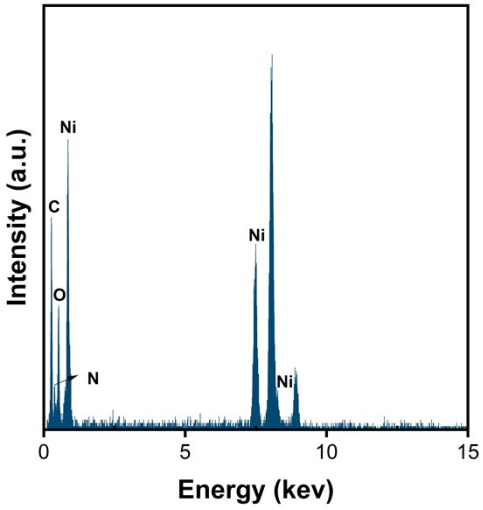

Figure S3. EDS spectra of Ni-Py-3-AO.

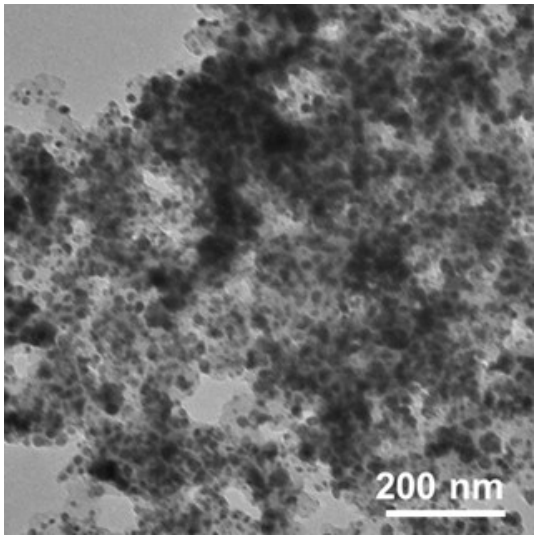

Figure S4. TEM image of Ni/C.

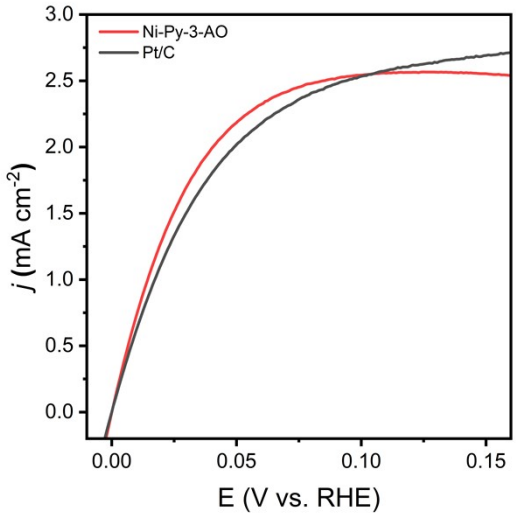

Figure S5. Polarization curves of Ni-Py-3-AO and commercial 20% Pt/C in H_2-saturated 0.1 M KOH with the rotation rate was 1600 rpm and the scan rate of 1 mV s^{-1}. The potentials were *iR* corrected.

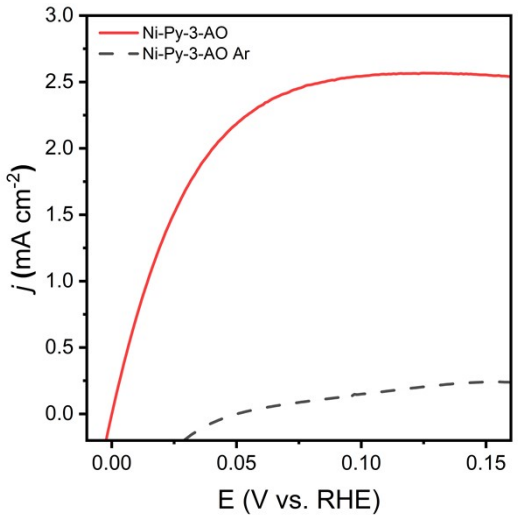

Figure S6. Polarization curves of Ni-Py-3-AO in H_2- and Ar-saturated 0.1 M KOH with the rotation rate was 1600 rpm and the scan rate of 1 mV s^{-1}. The potentials were *iR* corrected.

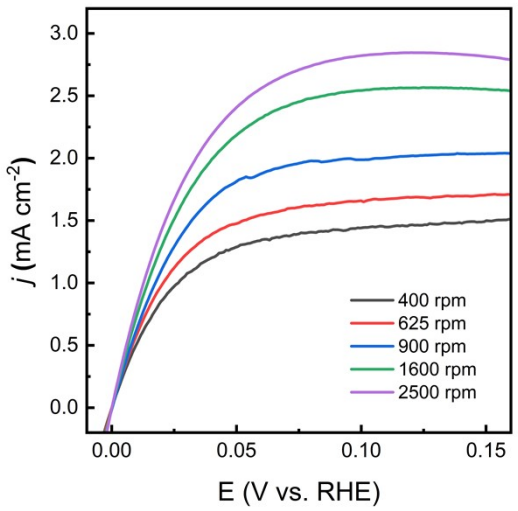

Figure S7. Polarization curves of Ni-Py-3-AO at different rotation rates in H_2-saturated 0.1 M KOH with the scan rate of 1 mV s^{-1}. The potentials were *iR* corrected.

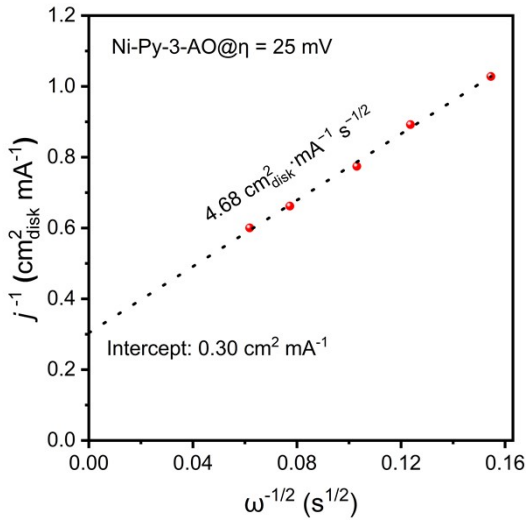

Figure S8. The corresponding Koutecky-Levich plot of Ni-Py-3-AO at 25 mV.

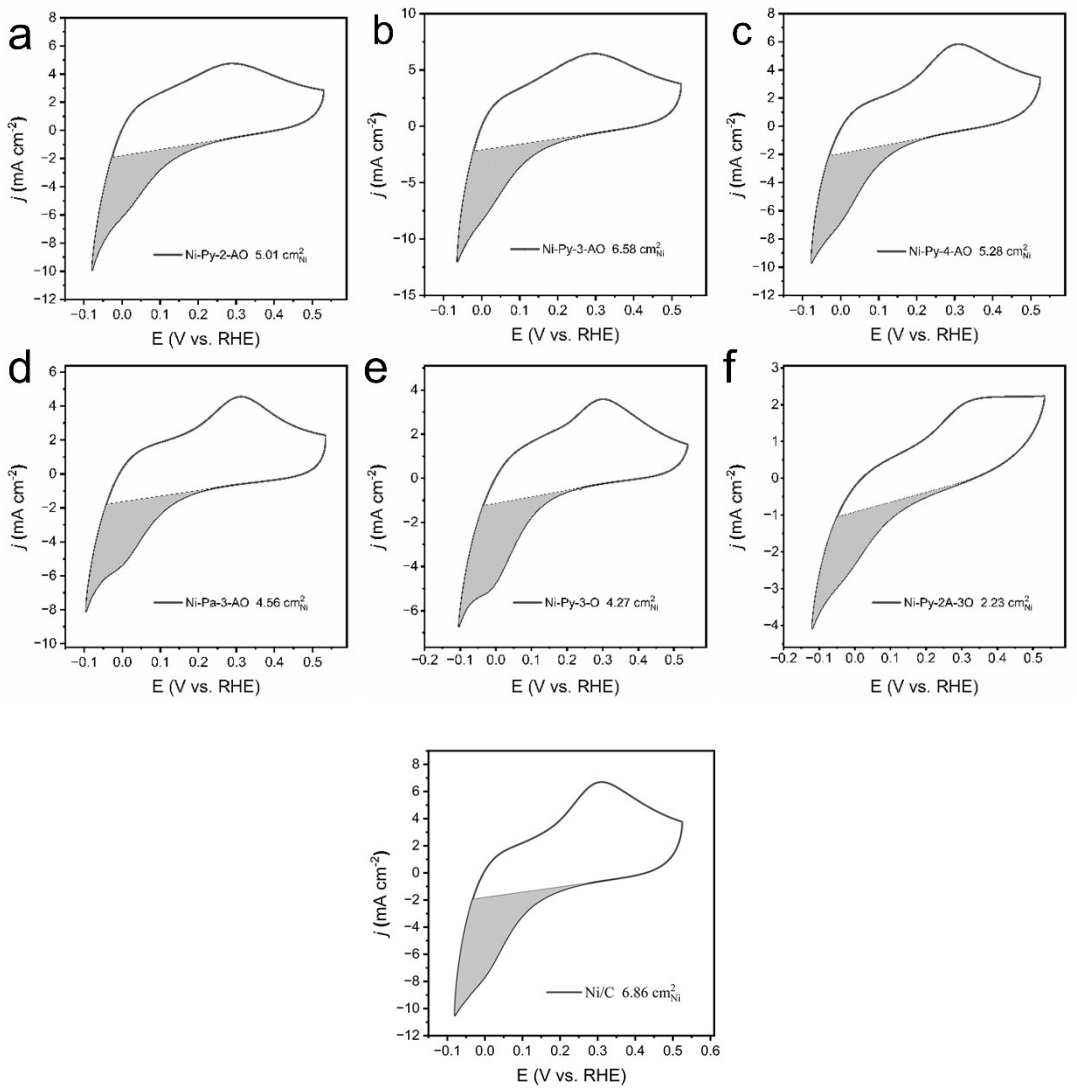

Figure S9. CV curves of Ni-Py-3-AO and other catalysts in Ar-saturated 0.1 M KOH with the rotation rate was 1600 rpm and the scan rate of 50 mV s^{-1}. The potentials were *iR* corrected.

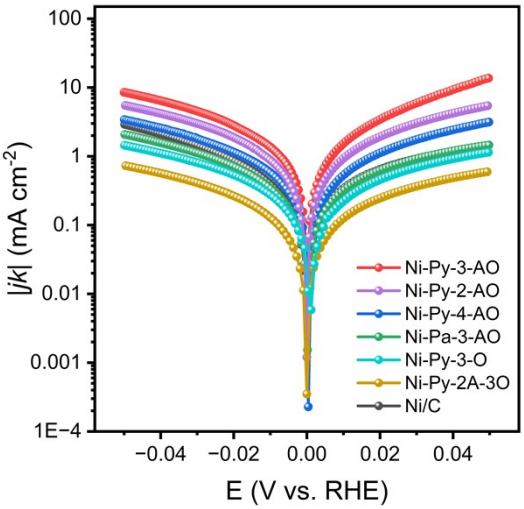

Figure S10. Tafel plots of the catalysts, where the current densities were normalized to disk area.

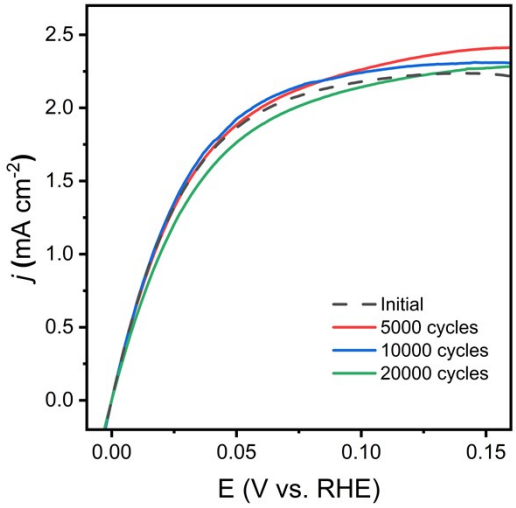

Figure S11. Polarization curves for Ni-Py-3-AO before and after ADT in H_2-saturated 0.1 M KOH with the rotation rate was 1600 rpm and the scan rate of 1 mV s^{-1}. The potentials were *iR* corrected.

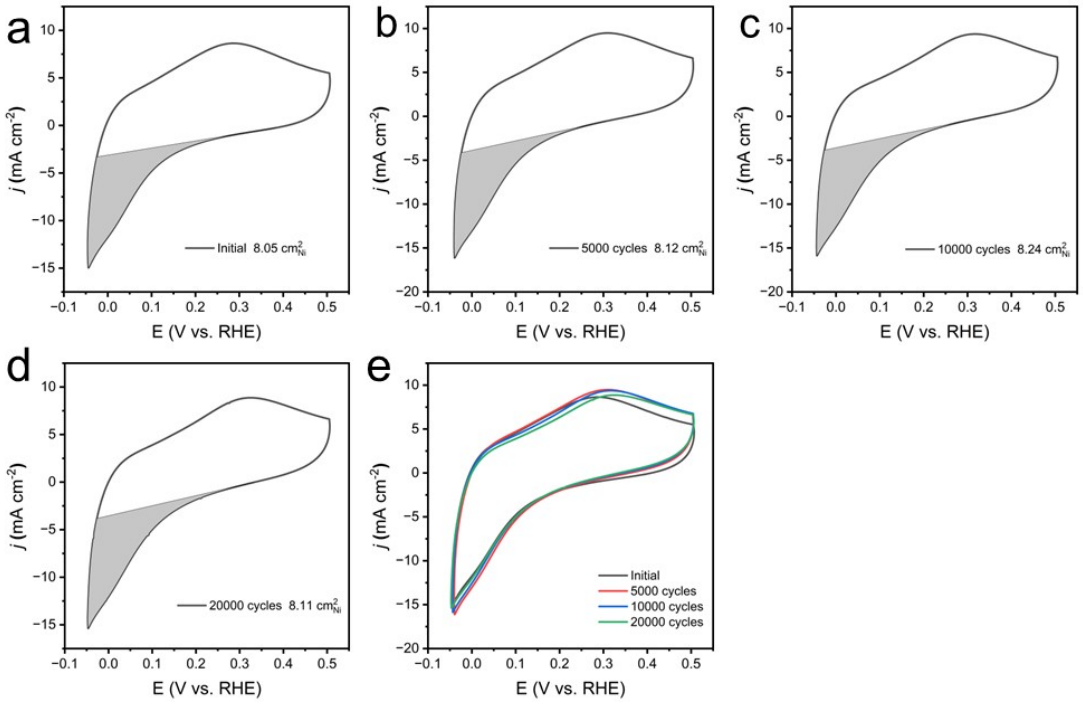

Figure S12. Polarization curves of Ni-3-Py-3-AO in ADT in Ar-saturated 0.1 M KOH with the rotation rate was 1600 rpm and the scan rate of 50 mV s^{-1}. The potentials were *iR* corrected.

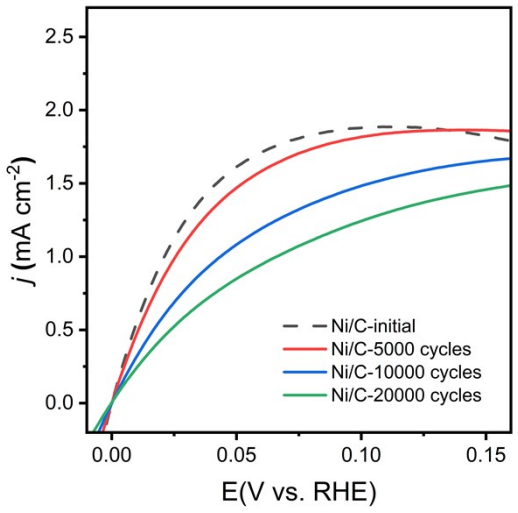

Figure S13. Polarization curves for Ni/C before and after ADT in H_2-saturated 0.1 M KOH with the rotation rate was 1600 rpm and the scan rate of 1 mV s^{-1}. The potentials were *iR* corrected.

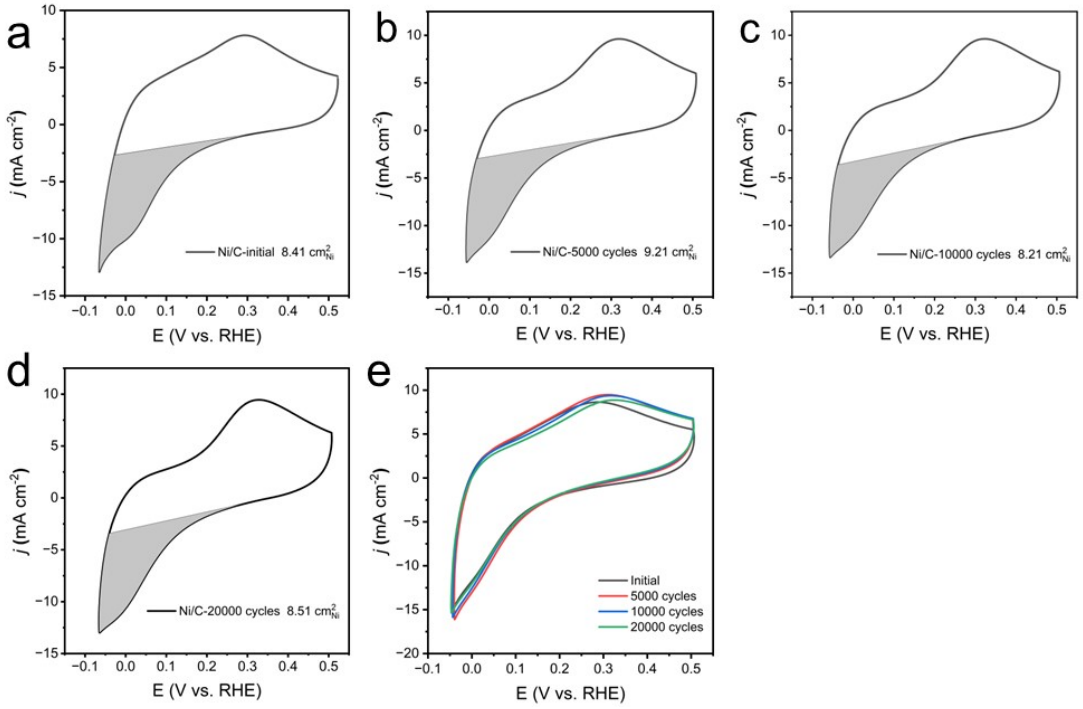

Figure S14. Polarization curves of Ni/C in ADT in Ar-saturated 0.1 M KOH with the rotation rate was 1600 rpm and the scan rate of 50 mV s^{-1}. The potentials were *iR* corrected.

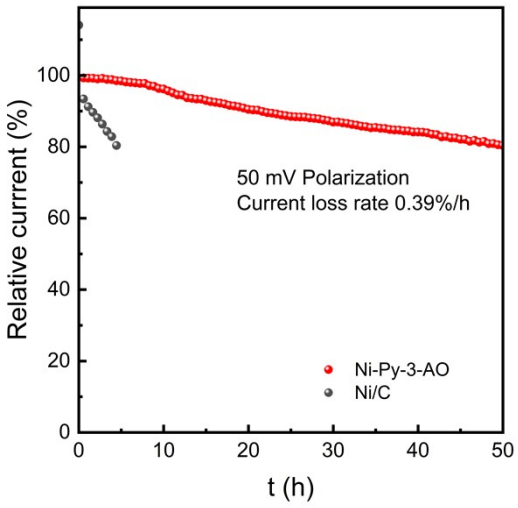

Figure S15. The chronoamperometry of Ni-Py-3-AO and Ni/C at 50 mV in H_2-saturated 0.1 M KOH with the rotation rate was 1600 rpm.

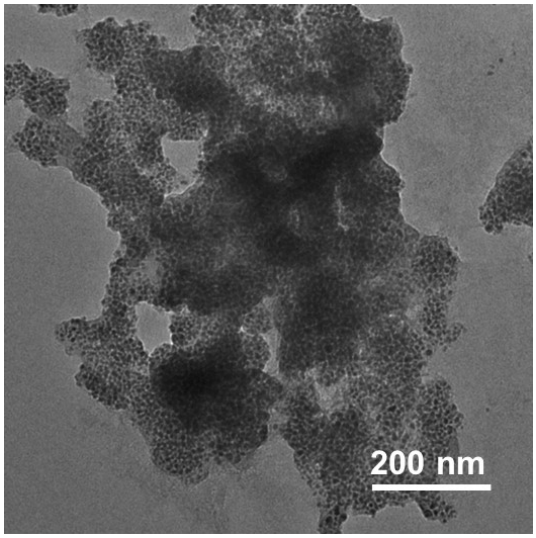

Figure S16. TEM of Ni-Py-3-AO after ADT.

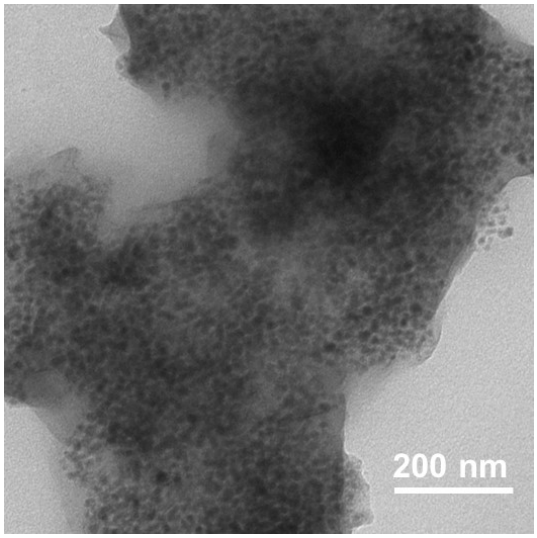

Figure S17. TEM of Ni-Py-3-AO after CA.

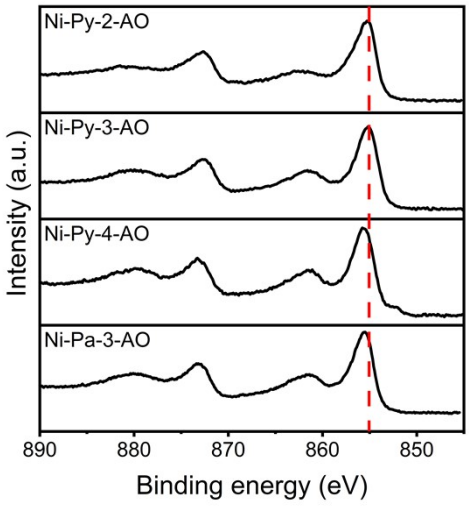

Figure S18. The high resolution Ni $2p^{3/2}$ XPS spectra of the precursors of Ni-Py-2-AO, Ni-Py-3-AO, Ni-Py-4-AO and Ni-Pa-3-AO.

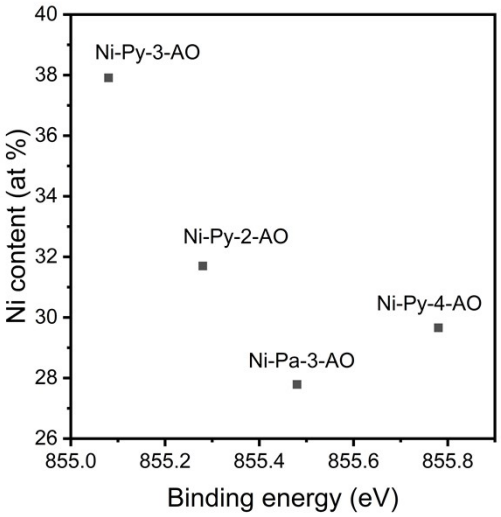

Figure S19. The relationship between the Ni binding energy of precursor and the resulting metallic Ni^0 content after pyrolysis.

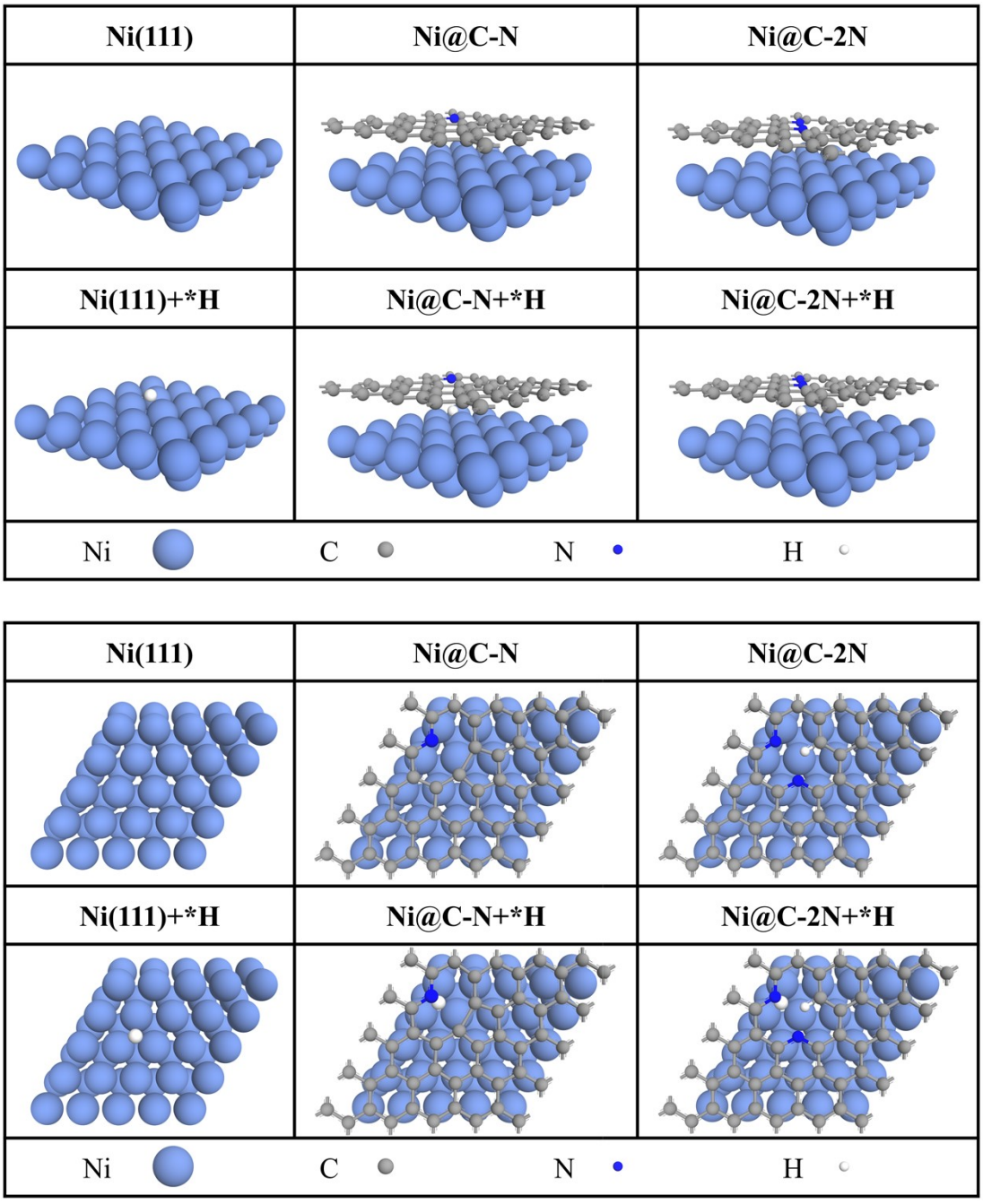

Figure S20. Side view (top) and top view (bottom) of the pristine and H adsorbed Ni(111), Ni@C-N and Ni@C-2N models.

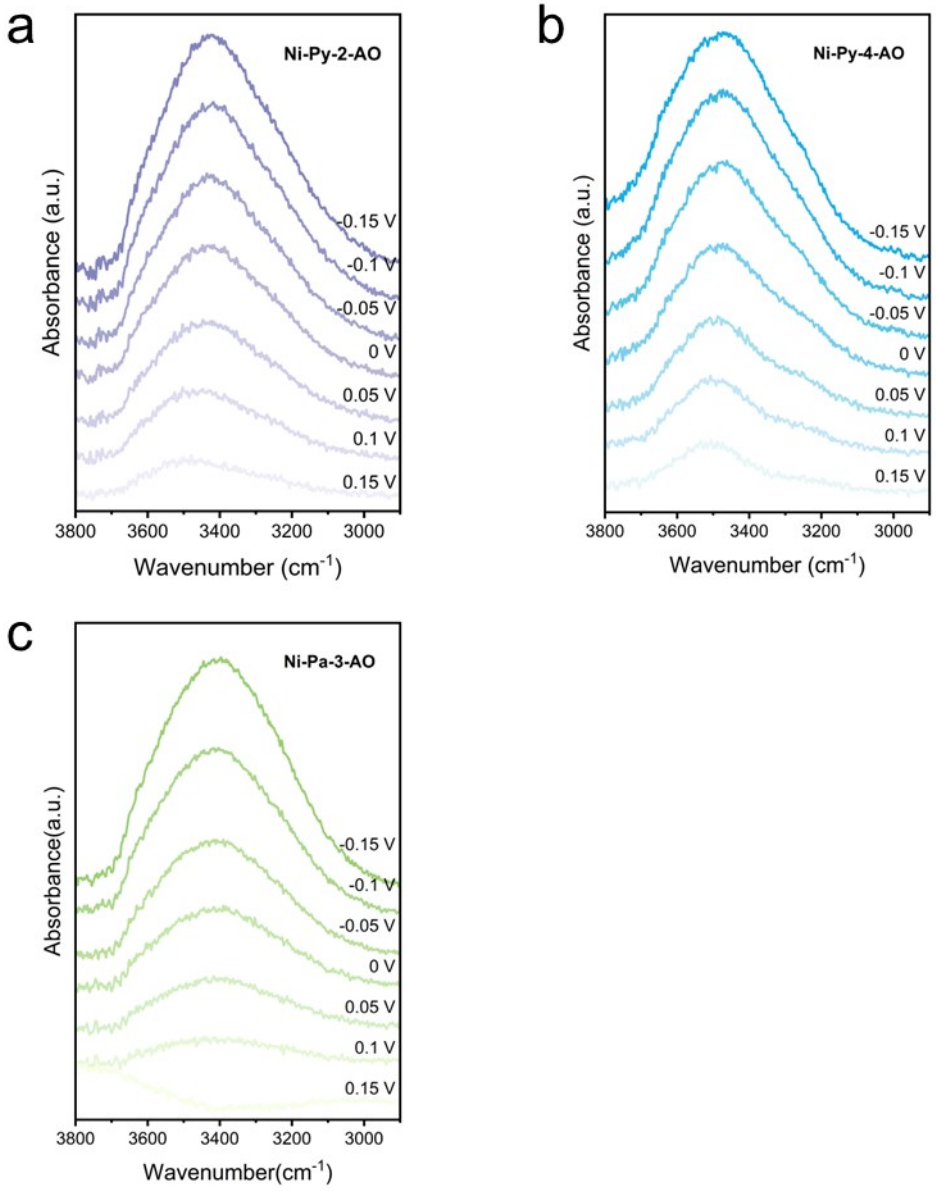

Figure S21. Electrochemical in situ ATR-SEIRAS of (a) Ni-Py-2-AO, (b) Ni-Py-4-AO and (c) Ni-Pa-3-AO. The measurement was carried out in H_2-saturated 0.1 M KOH. The background spectra were obtained at 0.2 V.

Table S1. The particle sizes measured from TEM and XRD.

Catalyst	Ni particle sizes (nm)	
	TEM	**XRD**
Ni-Py-2-AO	11.8	11.1
Ni-Py-3-AO	6.6	8.0
Ni-Py-4-AO	13.1	11.5
Ni-Pa-3-AO	9.4	11.8
Ni-Py-3-O	81	50
Ni-Py-2A-3O	13.3	13.4

Table S2. Summary of the HOR activity.

Catalyst	j_k at 50 mV (mA cm^{-2})	$j_{0,s}$ (μA·cm$^{-2}_{Ni}$)
Ni-Py-2-AO	5.4	97
Ni-Py-3-AO	13.8	138
Ni-Py-4-AO	3.1	55
Ni-Pa-3-AO	1.5	35
Ni-Py-3-O	1.1	27
Ni-Py-2A-3O	0.6	27
Ni/C	1.4	27

Table S3. Summary of HOR activity of Ni-based (Ni single metal) catalysts in the literature.

Catalyst	Electrolyte	$j_{0,s}$(μA·cm$_{Ni}^{-2}$)	$j_{k,m}$(A·g$_{Ni}^{-1}$)	Ref.
Ni-Py-3-AO	0.1 M KOH	138	94.1	This work
Ni@O_i-Ni	0.1 M KOH	72	85.63	[5]
Ni/Ni_3N-C	0.1 M KOH	36.45	12.18	[6]
Ni@NC/PEI-XC	0.1 M KOH	38	24.4	[7]
Ni-H_2-NH_3	0.1 M KOH	70	59.2	[8]
Ni-H_2-2%	0.1 M KOH	24.41	50.4	[9]
Ni/NiO/C700	0.1 M KOH	26	5.0	[10]
Ni_3N/C	0.1 M KOH	14	24.38	[11]
Ni/SC	0.1 M KOH	40.2	11.0	[12]
Ni/N-CNT	0.1 M KOH	28	9.3	[13]
4.3%N–Ni	0.1 M KOH	41	77.13	[14]
Ni_3N-r	0.1 M KOH	38	40.69	[15]
hcp/fcc-Ni-C	0.1 M KOH	30.88	12.28	[16]
Ch-activated Ni_{ED}/XC-72	0.1 M NaOH	56	32.1	[17]
Ni@C-500 °C	0.1 M KOH	32	-	[18]
C_{less}-Ni	0.1 M KOH	70	77	[19]
Ni-1% H_2/Ar	0.1 M KOH	90	-	[20]
Ni@BNC	0.1 M KOH	60.8	23.28	[21]
Ni-N_x@C	0.1 M KOH	60.90	74	[22]
Ni/TN-CNS-0.3	0.1 M KOH	30	-	[23]
Ni@BC	0.1 M KOH	45	34.91	[24]
Ni-400 ($NiO_{0.41}$)	0.1 M NaOH	18	-	[25]

Table S4. Summary of AEMFC performance of Ni-based (Ni single metal) catalysts in the literature.

Anode catalyst	Cathode catalyst	Cell temperature (°C)	Backpressure (anode/cathode, kPa)	Peak power density (mW cm^{-2})	Ref.
Ni-Py-3-AO	Pt/C	95	250/250	554	This work
Ni@Or-Ni	Pt/C	80	200/200	274	[5]
Ni/Ni_3N-C	Pt/C	80	200/200	222.5	[6]
Ni@NC/PEI-XC	Pt/C	80	200/200	241	[7]
Ni-H_2-NH_3	Pt/C	95	250/250	628	[8]
Ni@C-500 °C	Pt/C	80	200/200	160	[18]
Ni-1% H_2/Ar	Pt/C	80	200/200	670	[20]
Ni-N_x@C	Pt/C	80	100/100	203	[22]
Ni_3N	Pt/C	80	200/200	532	[26]
Ni@CN	Pt/C	80	200/200	66	[27]
Ni@CN_x	Pt/C	80	200/200	480	[28]

Reference

1 J. Hafner, *J. Comput. Chem.*, 2008, **29**, 2044–2078.
2 P. E. Blöchl, C. J. Först and J. Schimpl, *Bull. Mater. Sci.*, 2003, **26**, 33–41.
3 G. Kresse and D. Joubert, *Phys. Rev. B*, 1999, **59**, 1758–1775.
4 J. Rossmeisl, A. Logadottir and J. K. Nørskov, *Chem. Phys.*, 2005, **319**, 178–184.
5 Y. Men, X. Su, P. Li, Y. Tan, C. Ge, S. Jia, L. Li, J. Wang, G. Cheng, L. Zhuang, S. Chen and W. Luo, *J. Am. Chem. Soc.*, 2022, **144**, 12661–12672.
6 L. Su, D. Gong, N. Yao, Y. Li, Z. Li and W. Luo, *Adv. Funct. Mater.*, 2021, **31**, 2106156.
7 J. Wang, X. Dong, J. Liu, W. Li, L. T. Roling, J. Xiao and L. Jiang, *ACS Catal.*, 2021, **11**, 7422–7428.
8 W. Ni, T. Wang, F. Héroguel, A. Krammer, S. Lee, L. Yao, A. Schüler, J. S. Luterbacher, Y. Yan and X. Hu, *Nat. Mater.*, 2022, **21**, 804–810.
9 W. Ni, T. Wang, P. A. Schouwink, Y. Chuang, H. M. Chen and X. Hu, *Angew. Chem. Int. Ed.*, 2020, **59**, 10797–10801.
10 Y. Yang, X. Sun, G. Han, X. Liu, X. Zhang, Y. Sun, M. Zhang, Z. Cao and Y. Sun, *Angew. Chem. Int. Ed.*, 2019, **58**, 10644–10649.
11 W. Ni, A. Krammer, C. Hsu, H. M. Chen, A. Schüler and X. Hu, *Angew. Chem. Int. Ed.*, 2019, **58**, 7445–7449.
12 F. Yang, X. Bao, Y. Zhao, X. Wang, G. Cheng and W. Luo, *J. Mater. Chem. A*, 2019, **7**, 10936–10941.
13 Z. Zhuang, S. A. Giles, J. Zheng, G. R. Jenness, S. Caratzoulas, D. G. Vlachos and Y. Yan, *Nat. Commun.*, 2016, **7**, 10141.
14 X. Zhao, X. Li, L. An, K. Iputera, J. Zhu, P. Gao, R.-S. Liu, Z. Peng, J. Yang and D. Wang, *Energy Environ. Sci.*, 2022, **15**, 1234–1242.
15 X. Zhao, X. Li, L. An, L. Zheng, J. Yang and D. Wang, *Angew. Chem. Int. Ed.*, 2022, **61**, e202206588.
16 Y. Li, Z. Li, H. Cong, C. Yang, G. Cheng and W. Luo, *ACS Sustainable Chem. Eng.*, 2022, **10**, 3682–3689.
17 A. G. Oshchepkov, A. Bonnefont, S. N. Pronkin, O. V. Cherstiouk, C. Ulhaq-Bouillet, V. Papaefthimiou, V. N. Parmon and E. R. Savinova, *J. Power Sources*, 2018, **402**, 447–452.
18 Y. Gao, H. Peng, Y. Wang, G. Wang, L. Xiao, J. Lu and L. Zhuang, *ACS Appl. Mater. Interfaces*, 2020, **12**, 31575–31581.
19 J. He, L. Luo, J. Li, S. Chen, S. Yu, L. Zeng, Y. Wang and Y. Chen, *Angew. Chem. Int. Ed.*, 2025, **64**, e202423647.
20 R. Ren, C. Ge, Q. Li, G. Wang, L. Xiao, J. Lu and L. Zhuang, *J. Power Sources*, 2023, **556**, 232439.
21 J. Liu, W. Yu, M. Wang, J. Gao, X. Cui and L. Jiang, *ACS Catal.*, 2025, **15**, 4110–4120.
22 X. Wang, Y. Tong, X. Li, L. Zhao, Y. Cui, Y. Wang, H. Hu, T. Cai, M. Wu, H. Hu, Q. Xue, Z. Yan and W. Xing, *Chem. Eng. J.*, 2022, **445**, 136700.
23 S. Jiang, Q. Cheng, L. Zou, Z. Zou, Y. Li, Q. Zhang, Y. Gao and H. Yang, *Chem. Phys. Lett.*, 2019, **728**, 19–24.
24 P. Han, X. Yang, L. Wu, H. Jia and W. Luo, *Chem. Sci.*, 2024, **15**, 5633–5641.
25 C. Sun, P. Zhao, Y. Yang, Z. Li and W. Sheng, *ACS Catal.*, 2022, **12**, 11830–11837.

26 X.-L. Zhang, S.-J. Hu, Y.-H. Wang, L. Shi, Y. Yang and M.-R. Gao, *Nano Lett.*, 2023, **23**, 107–115.
27 X. Wang, J. Fang, X. Liu, D. Wei, Y. Yin, H. Wei, J. Zhang, Y. Zhang, X. Zhang, W. Zhu and Z. Zhuang, *Appl. Cata. B*, 2023, **327**, 122442.
28 Y. Gao, Y. Yang, R. Schimmenti, E. Murray, H. Peng, Y. Wang, C. Ge, W. Jiang, G. Wang, F. J. DiSalvo, D. A. Muller, M. Mavrikakis, L. Xiao, H. D. Abruña and L. Zhuang, *Proc. Natl. Acad. Sci. U.S.A.*, 2022, **119**, e2119883119.